

# Dynamics of Three Non-co-rotating Vortices in Bose-Einstein Condensates

V. Koukouloyannis and G. Voyatzis

*Department of Physics, University of Thessaloniki, GR-54124 Thessaloniki, Greece*

P.G. Kevrekidis

*Department of Mathematics and Statistics, University of Massachusetts, Amherst MA 01003-4515*

In this work we use standard Hamiltonian-system techniques in order to study the dynamics of three vortices with alternating charges in a confined Bose-Einstein condensate. In addition to being motivated by recent experiments, this system offers a natural vehicle for the exploration of the transition of the vortex dynamics from ordered to progressively chaotic behavior. In particular, it possesses two integrals of motion, the *energy* (which is expressed through the Hamiltonian  $H$ ) and the *angular momentum*  $L$  of the system. By using the integral of the angular momentum, we reduce the system to a two degree-of-freedom one with  $L$  as a parameter and reveal the topology of the phase space through the method of Poincaré surfaces of section.

We categorize the various motions that appear in the different regions of the sections and we study the major bifurcations that occur to the families of periodic motions of the system. Finally, we correspond the orbits on the surfaces of section to the real space motion of the vortices in the plane.

## I. INTRODUCTION

The exploration of 2D point vortex dynamics is a fascinating topic with a rich history for over a century, starting, arguably, with the fundamental contribution of Lord Kelvin [1] and gradually progressing to the consideration of higher numbers of vortices (see e.g. [2, 3]) and of not only symmetric but also of asymmetric equilibria thereof (see e.g. [4]). This large volume of relevant fluid literature extending from few vortex clusters to large scale vortex crystals has been summarized in numerous publications; see e.g. the review [5] and the book [6]. Along the way, this effort has also triggered experimental investigations considering not only stable vortex patterns in rotating superfluid  $^4\text{He}$  [7], but also electron columns confined in Malmberg-Penning traps [8] and even magnetized, millimeter sized disks rotating at a liquid-air interface [9]. Even from a theoretical viewpoint, this remains a highly active research front recently extending towards the consideration e.g. of relative equilibria of  $N+1$  vortices [10] and of vortex swarms [11].

On the other hand, over the last decade the consideration of vortex and multi-vortex states has had a novel focal point of attention and extensive applications, namely that of atomic Bose-Einstein condensates (BECs) [12–16]. In the latter setting, most of the consideration has been focused on the study of individual vortices and vortex lattices [12, 13, 16, 17]. However, clusters of few vortices have been of interest both theoretically [18] and experimentally [19] since the early days of BEC vortex experiments. Moreover, recent work on vortex dipoles created either via a quenching process through the phase transition [20–22] or through a superfluid flow past a cylinder experiment [23] and even studies of tripoles [22, 24] or higher core vortex clusters have sparked a considerable effort to understand the properties of such states. Notably, a fundamental twist, which is present in this setting in comparison to the earlier fluid ones, is the effect of an external, typically parabolic [14–16], trap inducing a precession of each of the vortices (with the direction depending on the sign of its charge). It is the delicate interplay of this precession with the vortex-vortex interaction which constitutes the source for numerous unexpected features in this system, such as the presence of neutral equilibria [21] for opposite charge vortices, or the symmetry-breaking bifurcation destabilizing symmetric same charge vortex states.

Our emphasis in the present work will be on the study of the so-called vortex tripole, a three-vortex configuration in which two of the vortices are of one charge, while the third is of the opposite charge. This configuration has been observed experimentally in the dynamics of [24] (see, in particular, Figs. 1b, 2b and 3 therein), which are the motivating starting point for the present considerations. Moreover, contrary to the two-vortex system, which has been argued in [21] to be integrable (at the particle level and near-integrable at the mean-field partial differential equation -PDE- level) in isotropic BECs, the three-vortex system is *generically* non-integrable. This is what offers, in turn, the theoretical motivation for the study. This setting provides one of the most elementary contexts, where the transition of the vortex dynamics from ordered states and stable periodic orbits to unstable ones and eventually to chaotic dynamics takes place. Our scope is to provide a systematic view toward this transition, using the integrals of the (vortex) motion as our control parameters. It turns out that when the motion is close to the one- or two-vortex regime the motion is usually regular, while if all of the vortices interact strongly with each other the motion is general chaotic.

Our presentation is structured as follows. In section II, we provide the details of the mathematical model used for the study of the system of interacting vortices and its Hamiltonian formulation. After that we provide the transformations needed in order to bring it to a reduced form, with its angular momentum  $L$  as a parameter. In section III, we proceed to the numerical study of our model by computing Poincaré sections and indicating particular bifurcations as our control parameter  $L$  is varied. In section IV, we will present a comparison of the ODE results of our reduced equations with the corresponding PDE results of the Gross-Pitaevskii equation (GPE) in order to examine the relevance of our findings based on the vortex particle model for the physical system of interest. Finally, in section V, we summarize our findings and present our conclusions and some future challenges.

## II. MATHEMATICAL MODEL OF THE SYSTEM OF INTERACTING VORTICES - HAMILTONIAN FORMULATION

As it has been illustrated in the earlier works of [21, 22], the reduction of the vortex dynamics from the original experiment to that of the mean-field PDE and from there to the “particle” ordinary differential equations (ODEs) works well in suitable quasi-two-dimensional (pancake-shaped) BECs with sufficiently large atom numbers. It is for that reason that, in what follows, we will restrict our considerations to the case of the ODE description of the motion of the vortex cores.

A single vortex in a harmonic trap is well-known to precess around the center of the trap [12, 13]. The frequency  $\omega_{\text{pr}}$  of the associated precession has been shown through suitable asymptotic considerations [12] (and more recently also through rigorous analysis [25]) to depend on the parameters of the system, such as the ratio of the trap frequencies in the radial and  $z$ -direction  $\Omega = \omega_r/\omega_z$  and the chemical potential  $\mu$ , which is directly associated with the atom number of the 2d isotropic BEC, as well as on the distance of the vortex from the center of the trap,  $r$ . An expression that has been argued [20] to yield a good match between theory and experiment (at least for vortices not very close to the “outer rim” of the condensate [22]) is of the form:

$$\omega_{\text{pr}} = \frac{\omega_{\text{pr}}^0}{1 - \frac{r^2}{R_{\text{TF}}^2}}, \quad (1)$$

where  $R_{\text{TF}} = \sqrt{2\mu}/\Omega$  is the so-called Thomas-Fermi radius, approximately characterizing the radial extent of the BEC;  $\omega_{\text{pr}}^0$  is the precession frequency at the trap center for which the expression  $\omega_{\text{pr}}^0 = \ln(A\frac{\mu}{\Omega})/R_{\text{TF}}^2$ , with  $A = 2\sqrt{2}\pi$ , has been argued to yield good agreement with both PDE direct simulations and linearization spectral analysis via the Bogolyubov-de Gennes equations [26].

On the other hand, in the absence of a harmonic trap, two interacting vortices will rotate around each other with a frequency of  $\omega_{\text{vort}} = B/r_{ij}^2$ , where  $r_{ij} = \sqrt{(x_i - x_j)^2 + (y_i - y_j)^2}$  is the distance between the vortices and  $B$  is a constant factor. In the realm of a homogeneous BEC,  $B = 2$ , while in the presence of the trap, a factor lower than the value of the homogeneous case, has been used [26] to emulate the more complex effect of the modulated density induced screening. A more detailed functional form (but bearing an integral kernel expression for the interaction) has been given in [27]. However, for the considerations herein, we will restrict ourselves to a constant  $B$ , following the earlier works of [21, 22], which accurately captured experimentally counter-rotating and co-rotating vortex dynamics, respectively, through such an approach. This approximation is valid for vortices that are sufficiently well-separated and thin-core (i.e., “particle-like”) so that their structure does not affect their inter-particle interaction.

Based on the above assumptions, let us now consider  $N$  interacting vortices. If  $(x_i, y_i)$  is the position of the  $i$ -th vortex, the corresponding equations of motion due to the other vortices and the harmonic trap are then given by [21, 22, 26]

$$\dot{x}_i = -S_i\omega_{\text{pr}}y_i - B \sum_{j=1, j \neq i}^N S_j \frac{y_i - y_j}{2r_{ij}^2}, \quad (2)$$

$$\dot{y}_i = S_i\omega_{\text{pr}}x_i + B \sum_{j=1, j \neq i}^N S_j \frac{x_i - x_j}{2r_{ij}^2}, \quad (3)$$

where  $S_i$  is the charge of the  $i$ -th vortex and  $N$  is the total number of interacting vortices.

We can further rescale time to the period of the single vortex precessing near the center of the trap and space is scaled to the Thomas-Fermi Radius according to:

$$t \mapsto \frac{t}{\omega_{\text{pr}}^0}, \quad x \mapsto xR_{\text{TF}}, \quad y \mapsto yR_{\text{TF}}. \quad (4)$$

Then, the resulting equations of motion read:

$$\begin{aligned} \dot{x}_i &= -S_i \frac{y_i}{1 - r_i^2} - c \sum_{j=1, j \neq i}^N S_j \frac{y_i - y_j}{r_{ij}^2} \\ \dot{y}_i &= S_i \frac{x_i}{1 - r_i^2} + c \sum_{j=1, j \neq i}^N S_j \frac{x_i - x_j}{r_{ij}^2}, \end{aligned} \quad (5)$$

where we have introduced the non-dimensional parameter

$$c = \frac{B}{2 \ln(A\frac{\mu}{\Omega})}. \quad (6)$$

For our unit charge vortices, this dynamical evolution can be acquired by the Hamiltonian

$$H = \frac{1}{2} \sum_{k=1}^N \ln(1 - r_k^2) - \frac{c}{2} \sum_{k=1}^N \sum_{j>k}^N S_k S_j \ln(r_{kj}^2) \quad (7)$$

through the canonical equations

$$\dot{x}_i = S_i \frac{\partial H}{\partial y_i}, \quad \dot{y}_i = -S_i \frac{\partial H}{\partial x_i}.$$

In what follows hereafter, we restrict our study to the case of interest, namely the tripole with two vortices of one circulation and one of opposite circulation. Vortices are assumed to be of unit charge, since these are generically stable, contrary to the unstable case for higher charges [28].

### A. The $N = 3$ , $S_1 = S_3 = 1$ , $S_2 = -1$ case

We will consider a system of  $N = 3$  interacting vortices, two with charge  $S_1 = S_3 = 1$  and one with charge  $S_2 = -1$ , as per the observations of [24]. According to (7), the Hamiltonian in this case will be

$$H = \frac{1}{2} \sum_{i=1}^3 \ln(1 - r_i^2) + \frac{c}{2} [\ln(r_{12}^2) - \ln(r_{13}^2) + \ln(r_{23}^2)],$$

where we recall that  $r_i = \sqrt{x_i^2 + y_i^2}$  and  $r_{ij} = \sqrt{(x_i - x_j)^2 + (y_i - y_j)^2}$ . If we define  $\mathbf{q} = (x_1, y_2, x_3)$  to be the *generalized positions* of the system and  $\mathbf{p} = (y_1, x_2, y_3)$  to be the conjugate *generalized momenta*, the corresponding equations of motion (5) are derived through the standard Hamilton's canonical equations

$$\dot{q}_i = \frac{\partial H}{\partial p_i}, \quad \dot{p}_i = -\frac{\partial H}{\partial q_i}.$$

**Remark:** Let  $\boldsymbol{\eta} = (\mathbf{q}, \mathbf{p})^T = (x_1, y_2, x_3, y_1, x_2, y_3)^T$ . Then the equations of motion can be written as

$$\dot{\boldsymbol{\eta}} = \boldsymbol{\Omega} D_{\boldsymbol{\eta}} H,$$

where  $\boldsymbol{\Omega}$  is the standard matrix of the symplectic structure  $\boldsymbol{\Omega} = \begin{pmatrix} \mathbf{O} & \mathbf{I} \\ -\mathbf{I} & \mathbf{O} \end{pmatrix}$ , with  $\mathbf{I}$  and  $\mathbf{O}$  being the  $3 \times 3$  identity and zero matrices respectively. By  $D_{\boldsymbol{\eta}}$  we denote the  $(\partial/\partial\eta_1 \dots \partial/\partial\eta_6)^T$  operator. Note that, one could use a different arrangement of variables, say  $\boldsymbol{\eta}'$ . The system would still have a Hamiltonian structure but with a different symplectic matrix  $\boldsymbol{\Omega}'$ . We choose the above mentioned arrangement of variables because it is convenient for the computation of the Poincaré sections.

### B. The reduced Hamiltonian

The Hamiltonian of the system can be reduced to a two-degree of freedom one, by applying two canonical transformations (i.e. transformations which preserve the functional form of the equations of motion). The first transformation concerns the rewriting of the Hamiltonian using the Poincaré variables  $(w_i, R_i)$ , which are defined by

$$q_i = \sqrt{2R_i} \sin(w_i), \quad p_i = \sqrt{2R_i} \cos(w_i). \quad (8)$$

Then, the Hamiltonian of the system becomes

$$\begin{aligned} H = & \frac{1}{2} [\ln(1 - 2R_1) + \ln(1 - 2R_2) + \ln(1 - 2R_3)] + \\ & + \frac{c}{2} \left[ \ln(2R_1 + 2R_2 - 4\sqrt{R_1 R_2} \sin(w_1 + w_2)) - \ln(2R_1 + 2R_3 - 4\sqrt{R_1 R_3} \cos(w_1 - w_3)) + \right. \\ & \left. + \ln(2R_2 + 2R_3 - 4\sqrt{R_2 R_3} \sin(w_2 + w_3)), \right] \end{aligned}$$

where the  $R_i$ 's must satisfy  $R_i < 0.5$ , which is tantamount to the vortices being located within the Thomas-Fermi radius. From the form of the transformed Hamiltonian it is obvious that the proper variables to use are not  $w_i$  but linear combinations thereof. So, we apply a second canonical transformation

$$\begin{aligned} \phi_1 &= w_1 - w_3 & J_1 &= R_1 \\ \phi_2 &= w_2 + w_3 & J_2 &= R_2 \\ \vartheta &= w_3 & L &= R_1 - R_2 + R_3. \end{aligned} \quad (9)$$

In this new set of variables,  $J_1$ ,  $J_2$ ,  $L$  are the conjugates of  $\phi_1$ ,  $\phi_2$ ,  $\vartheta$  respectively and have the specific chosen form in order for the transformation to be canonical. The variables  $\phi_1$ ,  $\phi_2$  can be considered as *generalized phase differences* (which differ from the standard ones because of the sign of  $S_2 = -1$ ) while  $\vartheta$  can be considered as the *phase* of the system. Since  $\vartheta$  is an angle variable, its conjugate variable  $L$  is the corresponding *angular momentum*. In general, the angular momentum for a vortex system is defined as  $L = \sum_i S_i r_i^2$  [5, 6], which, by using (8), coincides with the one in (9) and can be shown via direct computation to be a conserved quantity for the dynamical system associated with Eqs. (2)-(3).

By using the above mentioned transformation the Hamiltonian becomes

$$\begin{aligned}
 H = & \frac{1}{2} [\ln(1 - 2J_1) + \ln(1 - 2J_2) + \ln(1 - 2(L - J_1 + J_2))] \\
 & + \frac{c}{2} \left[ \ln(4J_2 - 2J_1 + 2L - 4\sqrt{J_2}\sqrt{L - J_1 + J_2} \sin(\phi_2)) - \ln(2L + 2J_2 - 4\sqrt{J_1}\sqrt{L - J_1 + J_2} \cos(\phi_1)) \right. \\
 & \left. + \ln(2J_1 + 2J_2 - 2\sqrt{J_1}\sqrt{J_2} \sin(\phi_1 + \phi_2)) \right].
 \end{aligned} \tag{10}$$

Since the variable  $\vartheta$  is ignorable (it is not explicitly contained in the Hamiltonian), the corresponding variable  $L$  is, as expected, an integral of motion. So, the system is transformed into a 2 degrees-of-freedom Hamiltonian system with the angular momentum  $L$  as a parameter. Since it appears that no other integral of motion exists (in addition to the  $H$  and  $L$ ), the Hamiltonian (10) is non-integrable. It is evident that the system represents the simplest non-integrable dynamical variant within an isotropic two-dimensional BEC. Thus, it is expected that regular and chaotic motion will coexist in the phase space of the system. So, the natural consideration is to study the transition of the dynamics from completely regular to progressively chaotic<sup>1</sup>, as parameters, such as the angular momentum  $L$ , are varied. For two degree-of-freedom systems, the Poincaré sections are the most illustrative tool for the investigation of the underlying dynamics.

### III. PHASE SPACE EXPLORATION THROUGH POINCARÉ SECTIONS.

We will study the dynamical behavior of this tripole system by using a sequence of Poincaré sections. A Poincaré section is defined for a fixed value of the energy of the system, which could be determined by some particular initial conditions of the motion, i.e.  $h = H(x_{10}, y_{10}, x_{20}, y_{20}, x_{30}, y_{30})$ . So, in order to span different relative position settings for the vortices of energy  $h$ , we will consider various values of the angular momentum  $L$ , which is used as a constant parameter for each section. In our numerical computations, the value of the energy has been chosen to be  $h = -0.7475$ , which corresponds to a typical initial configuration of the vortices as it is shown in Fig. 2. On the other hand, as it can be shown from (9) and by the fact that  $R_i$  lie in the range  $0 < R_i < 0.5$  we conclude that  $L$  can vary in the range  $-0.5 < L < 1$ . But, since there is the energy constraint as well, this range will be actually smaller.

For the surface of section we consider the  $(\phi_1 - J_1)$  plane and fix the value of  $\phi_2$  to be  $\phi_2 = \pi/2$ . This value of  $\phi_2$  corresponds to the state where the  $S_2$  and  $S_3$  vortices lie on the half-line having the center of the condensate on its edge as it can be seen from the transformations (8) and (9). Then, the value of  $J_2$ , for a given pair of  $\{\phi_1, J_1\}$  on the plane, can be inferred by solving the equation  $h = H(\phi_1, J_1, \phi_2, J_2, L)$ .

It is reminded here that, in general, isolated (fixed or periodic) points on the surface of section correspond to periodic orbits of the particular dynamical system. Similarly, invariant curves in the Poincaré sections will correspond to quasi-periodic orbits. But, this applies to the “reduced” phase-space of the  $\{\phi_1, \phi_2, J_1, J_2\}$  variables. In the present setting we have eliminated the third degree of freedom, by using the angular momentum integral  $L$ . This additional “hidden” degree of freedom introduces an extra frequency which is not necessarily commensurate with the frequencies of the other two degrees of freedom. As a result, a fixed point of the Poincaré section does not correspond, in general, to a periodic orbit in the  $(x-y)$  coordinates of the “full” system but to a *quasi-periodic* one. As we embark on a detailed analysis of the different orbits, this additional complication (bearing an additional frequency for each orbit to those “normally” counted on the basis of the Poincaré section) should be borne in mind. Moreover, the term

---

<sup>1</sup> Note here that a Hamiltonian system can never exhibit completely chaotic behavior since there are always islands of regularity in its phase space.

orbit is used in order to describe a trajectory in three different spaces; the full  $(x - y)$  phase-space, the reduced  $\{\phi_1, \phi_2, J_1, J_2\}$  phase-space and the  $(\phi_1 - J_1)$  surface of section. But, the distinction between them should be clear depending on the context.

### A. The regular motion region ( $L < L^*$ )

For all  $L < -0.218 = L^*$  the basic dynamical behavior is essentially invariant. In Fig. 1 we show the Poincaré section for  $L = -0.25$  as a representative of this regime of angular momenta. In this figure we can distinguish two regions. The first region consists of regular (quasi-periodic) orbits around the central periodic orbit with coordinates  $(\phi_1, J_1) \simeq (\pi, 0.063)$ . This region corresponds to the “rotational” regime where all three vortices rotate around the center of the condensate, each one having the rotation direction which is determined by its corresponding charge (counter-clockwise for the positive charges, clockwise for the negative charge). As regards the periodic orbit at  $(\phi_1, J_1) \simeq (\pi, 0.063)$ , its true quasi-periodic nature in the  $(x - y)$  plane is revealed in Fig. 2, where it is evident that it does not repeat itself, but instead covers densely a specific area of the plane. Furthermore, such orbits where  $\phi_2 = \pi/2$  and  $\phi_1 = \pi$  correspond to configurations having all the vortices aligned with the rotation center and having the  $S_2, S_3$  vortices on the opposite side of  $S_1$ . This kind of configurations will be called *symmetric* in what follows.

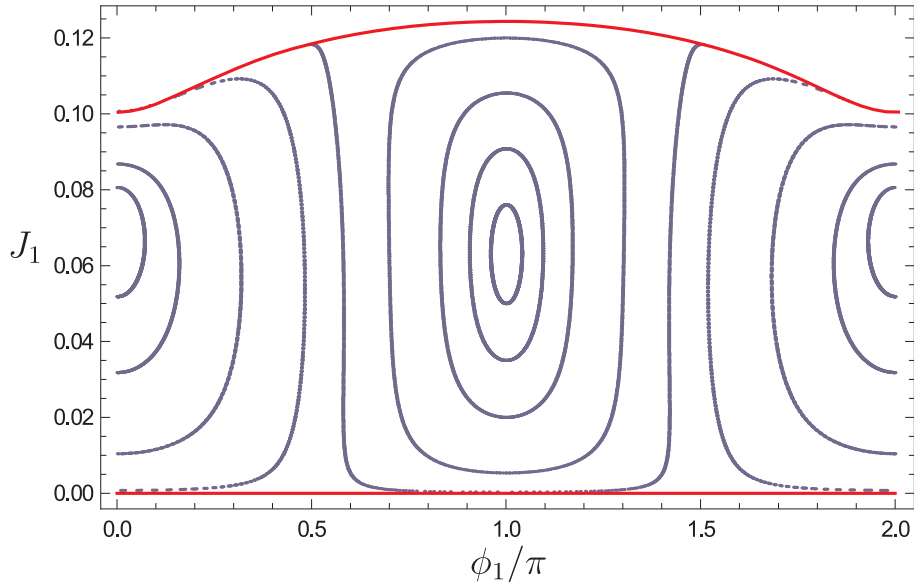


FIG. 1. (Color Online) The Poincaré section for  $L = -0.25$ . We can distinguish two regions of predominantly ordered dynamics, as discussed in detail in the text. The red (light colored) lines depict the boundaries of motion.

The second distinct region of motion in the Poincaré section is the set of regular orbits around  $(\phi_1, J_1) \simeq (0, 0.07)$ . Note that, since  $\phi_1$  is cyclic, the topology of the section is cylindrical and not flat. One could have expected this point to correspond to a periodic orbit, since it is surrounded by quasi-periodic orbits, but instead a *collision* between the  $S_1$  and  $S_3$  vortices occurs. The motion on the  $(x - y)$  plane of a characteristic orbit  $((\phi_1, J_1) \simeq (0.1, 0.03))$  in this area is shown in Fig. 3. This region corresponds to the motion where the  $S_1$  and  $S_3$  particles rotate around each other and both of them around the center. Such kind of motion is characterized as the “satellite” regime and constitute a very good representative of the two-vortex regime which is discussed in section III D.

In Fig. 1, there are also two red curves which represent the boundaries of the Poincaré section and correspond to the configurations in which one of the vortices is located at the center of the rotation. The shape of these curves is calculated by using the requirement of the suitable vortex to have  $R = 0$ . In particular, in the section of Fig. 1 we have used the conditions  $R_1 = 0$  and  $R_3 = 0$ . This is because, as it can be seen by the transformations (8) and (9), the positive contribution to  $L$  is related to  $R_1$  and  $R_3$ , while the negative contribution comes from  $R_2$ . Since the section of Fig. 1 corresponds to a low value of  $L$  ( $L = -0.25$ ), it means that the  $S_1$  and  $S_3$  vortices are moving close to the center of rotation. More specifically, the lower limit is calculated by considering  $R_1 = J_1 = 0$  while for the upper boundary we

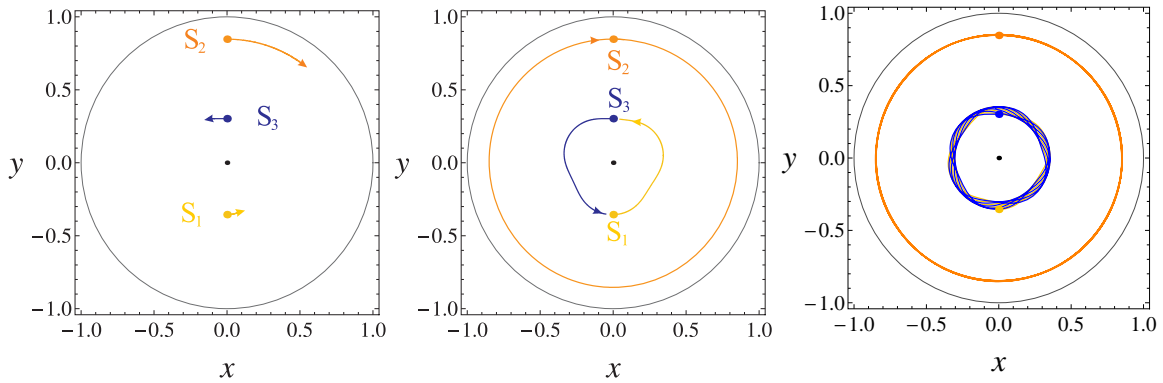


FIG. 2. (Color Online) An orbit in the  $(x - y)$  space for  $L = -0.25$  is shown. It corresponds to the “central” periodic orbit of Fig.1, which in turn represents a quasi-periodic orbit in the  $(x - y)$ -space. Here it is shown for three values of the time,  $t = 0.2$ ,  $t = 1.9$ ,  $t = 20$ , from left to right. The dots are showing the initial configuration. The yellow, orange and blue (light, intermediate and dark grey) dots correspond to the  $S_1$ ,  $S_2$  and  $S_3$  vortices respectively. The same same colors are used to the solid lines which denote the corresponding trajectories. The black dot represents the center of the condensate, while the gray circle represents the Thomas-Fermi radius.. This color code will be followed for the rest of this work. In addition, in the first two panels there are arrows indicating the main rotation direction of the vortices which is dictated by the gyroscopic precession due to the trapping potential.

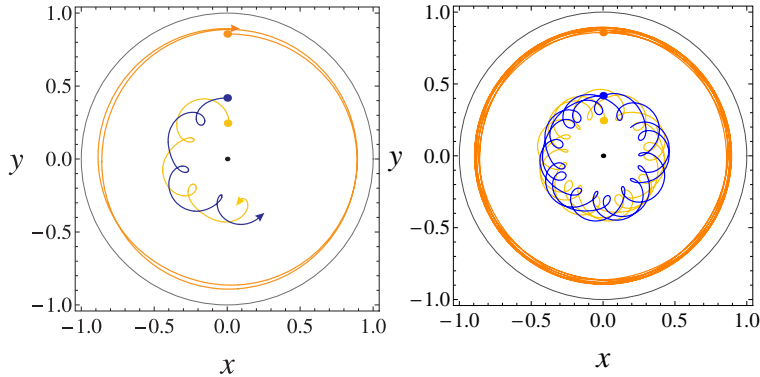


FIG. 3. (Color Online) An orbit for  $L = -0.25$  is shown which is a representative of the “satellite” regime orbits. It corresponds to  $(\phi_1, J_1) \simeq (0, 0.03)$  and it is depicted for  $t = 3$  (left panel) and  $t = 10$  (right panel).

consider  $R_3 = 0$  which leads to  $J_2 = J_1 - L$ . By inserting the last relationship in Eq. (10) as well as the fixed values of  $h$ ,  $L$  and  $\phi_2 = \pi/2$  we get the implicit formula for the function  $J_1 = J_1(\phi_1)$  of the upper boundary.

When the orbit of a vortex passes through the origin, the corresponding invariant curve on the Poincaré section collides with the boundary at a point  $(\phi_1, J_1) = (\phi^*, J^*)$ . At this point the angle  $w$  of the corresponding vortex undergoes a discontinuous change which implies a discontinuous change of the invariant curve which continues at the point  $(\phi_1, J_1) = (2\pi - \phi^*, J^*)$ . Although the true motion is not interrupted, the corresponding invariant curve in the Poincaré section appears disconnected, which is an artifact of the particular transformation (8) we have used. These specific orbits, which collide with the boundary, act as “separatrices”, distinguishing the rotational and satellite regimes.

On the other hand, the boundaries describe the upper and lower limits of the values of  $J_1$  which correspond to the extreme values the distance  $R_1$  can acquire satisfying also the constraint of the fixed value of  $L$ .

### B. The $L^* < L \leq 0$ region

The first structural change in the Poincaré sections occurs for  $L \simeq -0.218$ , where the “central” stable periodic orbit is replaced by one unstable and two stable through a supercritical “pitchfork” (i.e., spontaneous symmetry breaking) bifurcation as shown in Fig. 4. The top panel of the figure shows the location of the fixed points of the Poincaré section, rendering evident the nature of the bifurcation; this change

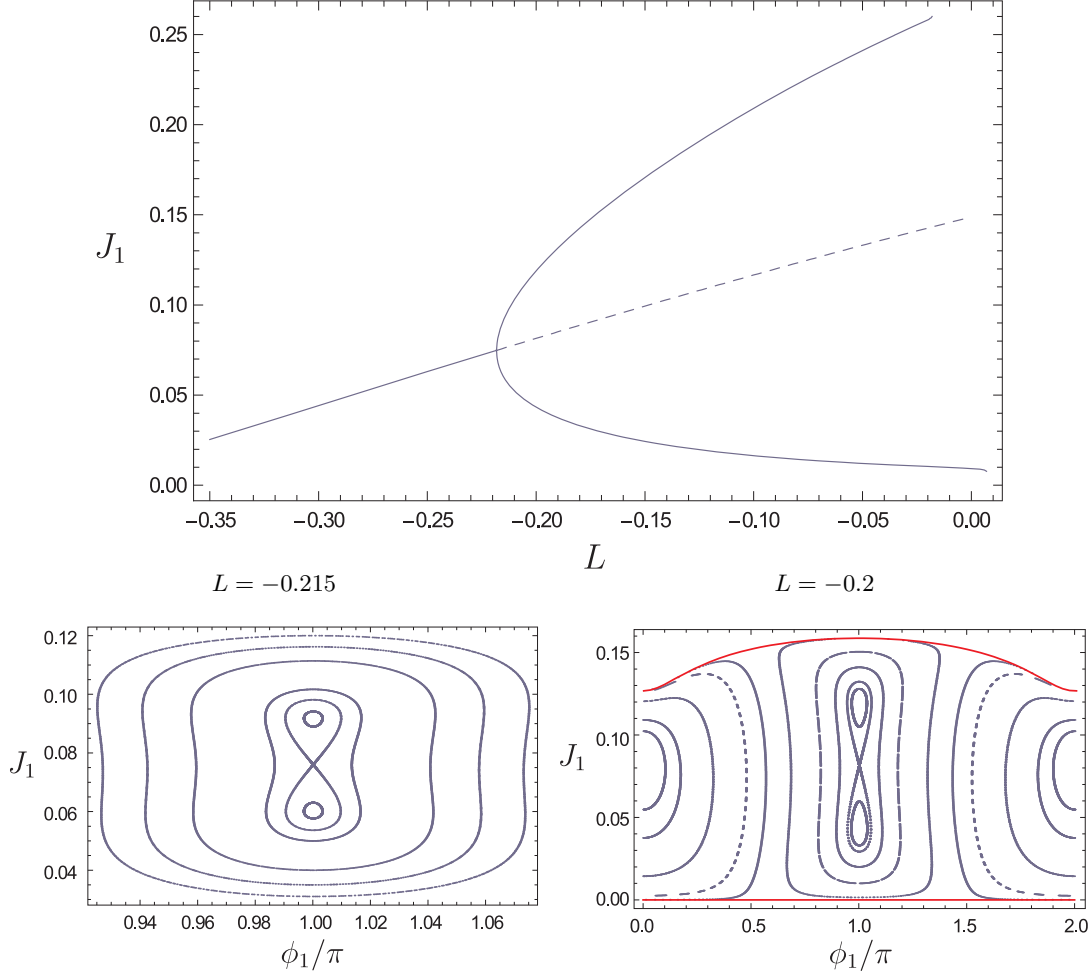


FIG. 4. (Color online) At  $L = -0.218$  a supercritical pitchfork bifurcation occurs, replacing the central stable periodic orbit with an unstable and two stable ones. In the diagram the value of  $J_1$  of these orbits on the section is shown as a function of  $L$ . The value of  $\phi_1$  is constant and equal to  $\phi_1 = \pi$ , i.e. all of them are symmetric (in the meaning of the term indicated above for vortex orbits considered herein). The Poincaré section of the system after the first pitchfork bifurcation which occurs for  $L \simeq -0.218$  is shown in the bottom panels of the figure. The left panel corresponds to a magnification of the section for  $L = -0.215$  around  $\phi_1 = \pi$ . In the right panel we show the full section for  $L = -0.2$ .

in the form of the surface of section is illustrated in the bottom panels of the figure. In the left panel a magnification of the section for  $L = -0.215$  around  $\phi_1 = \pi$  is depicted in order for the bifurcation to be shown. We can clearly see that the “central” stable periodic orbit is replaced by an unstable saddle point while two stable symmetric periodic orbits appear as well. The two stable configurations which correspond to  $(\phi_1, J_1) \simeq (\pi, 0.06)$  and  $(\phi_1, J_1) \simeq (\pi, 0.0918)$  are shown in the  $(x - y)$  space in the top panels of Fig. 5. As we can see, the two configurations are almost mirror images of each other, with the left-hand one having  $S_1$  orbiting more closely to the center than  $S_3$ , while in the right-hand panel the situation is reversed. In the bottom panels of Fig. 5 the unstable (symmetric) periodic orbit for  $(\phi_1, J_1) \simeq (\pi, 0.076)$  is depicted. In particular, its time evolution for  $t = 2.1$  and  $t = 20$  is shown. In these plots we can see that the area that the orbits of the vortices in the  $(x - y)$  plane are occupying is very narrow, almost one-dimensional. This indicates that the unstable orbit is very close to an “exact” periodic orbit of the full

system, which actually occurs for  $L \simeq -0.213$ . In the right panel of Fig. 4, the full section for  $L = -0.2$  is depicted. This also serves to illustrate that although the picture in the central region has changed, the region around the edges remains qualitatively similar as before the bifurcation.

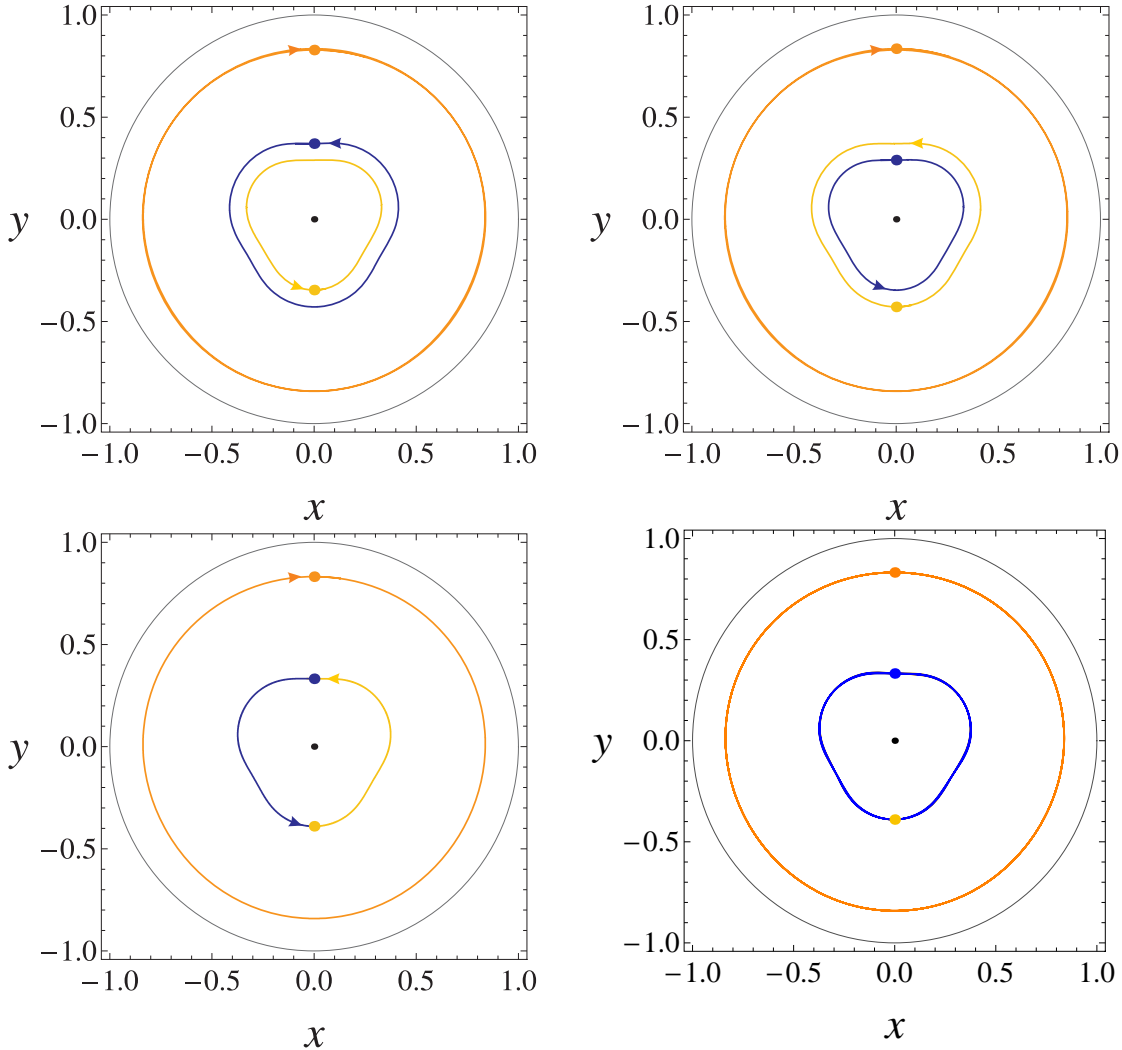


FIG. 5. (Color online) Top panels: the two stable periodic orbit configurations for  $L = -0.215$ , for  $t = 2.1$ . The two orbits are similar. In the one in the left panel which corresponds to  $(\phi_1, J_1) \simeq (\pi, 0.06)$  the  $S_1$  vortex rotates closer to the center than  $S_3$ , while in the configuration of the right panel, which corresponds to  $(\phi_1, J_1) \simeq (\pi, 0.0918)$  the situation is reversed. Bottom panels: the motion of the vortices which corresponds to the central unstable periodic orbit for  $L = -0.215$ . In the left panel the evolution for  $t = 2.1$  is shown while in the right hand panel the system has evolved for  $t = 20$ . As we can see the orbits of the vortices lie in an almost one-dimensional subspace of the  $(x - y)$  plane, indicating that this orbit is very close to the “exact” periodic orbit.

As the value of  $L$  is increasing, we can see in Fig. 6 that the saddle point associated with the unstable periodic orbit is replaced by a small chaotic region around it, which becomes wider as  $L$  becomes larger. I.e., the chaos, as may be expected [29] “emerges” from this saddle point and gradually expands there-around. In addition we can observe the splitting of some of the invariant curves to form Poincaré-Birkhoff chains [29] of islands (e.g. for  $L \geq -0.05$ ). In the center of these islands there are periodic orbits, which correspond to asymmetric configurations i.e. configurations with non-collinear initial conditions. Moreover, we observe the existence of islands of regularity inside the chaotic region, e.g. for  $L = 0$ . At this point we would like to stress that in our study the classification of the trajectories as regular or chaotic seems more meaningful from a physical point, since periodic trajectories are isolated and their periodicity refers only to the reduced model. Actually, as we mentioned before, stable periodic trajectories correspond to regular quasi-periodic orbits in the  $(x - y)$  plane for the vortices.

Nevertheless, the partition of ordered vs. chaotic regions on the sections can be clearly discerned within

the increasing  $L$  diagrams of Fig. 6. The chaotic region originating from the saddle point gradually expands along the direction of the former stable and unstable manifold of the saddle, overtaking the plane of the Poincaré section and gradually increasingly restricting the ordered regions thereof. The latter become progressively confined around the top and bottom periodic and the collision orbit of the outer (left and right) regions of this cylindrical space.

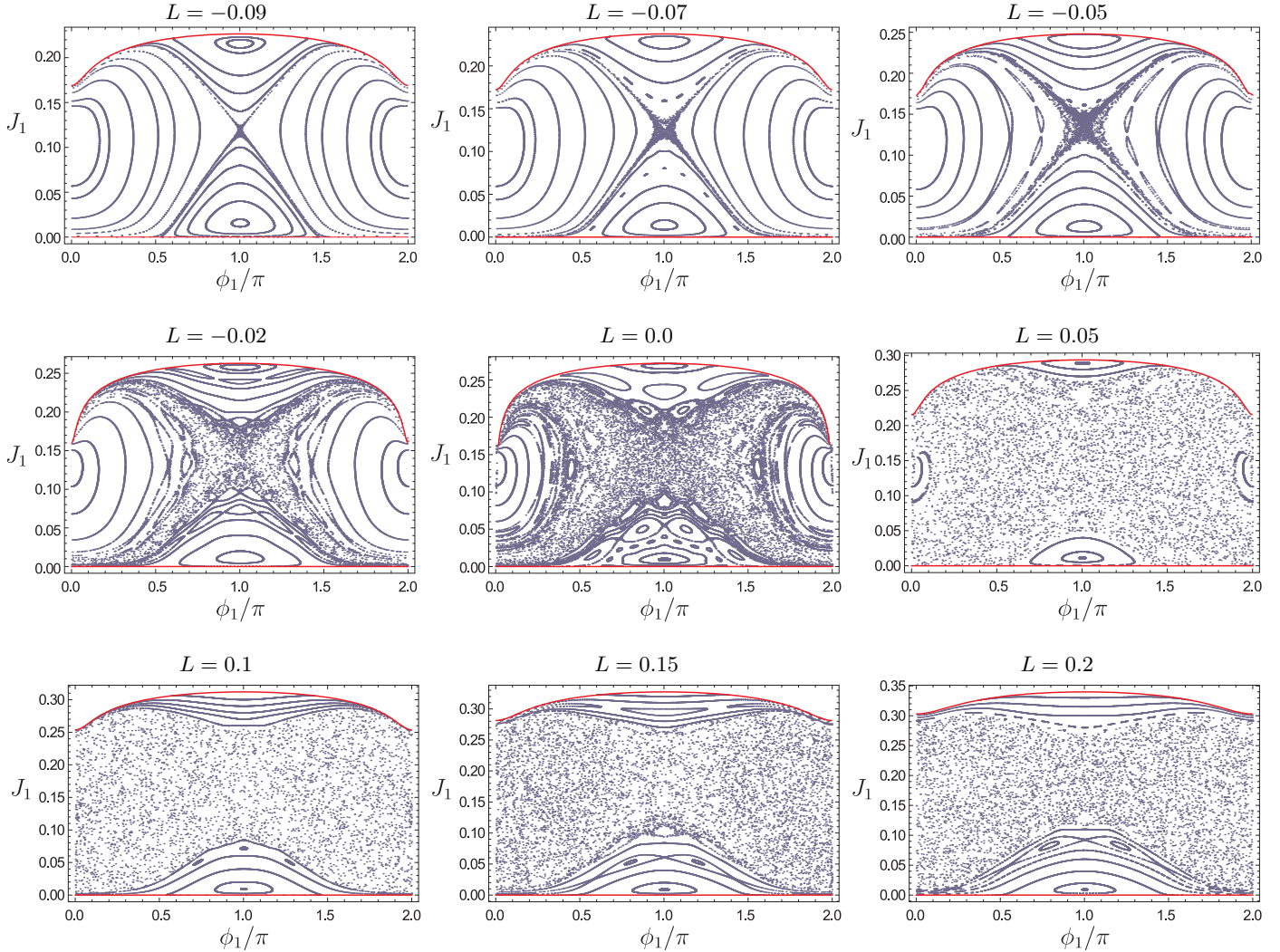


FIG. 6. (Color online) The graphs show the Poincaré section of the tripole system in the same format as e.g. in Fig. 1 but for the case of progressively increasing  $L$  in the range  $-0.09 \leq L \leq 0.2$ . As can be observed, the small chaotic region around the unstable central periodic orbit increases and finally spreads to almost all the phase space as the value of  $L$  is increased, while ordered dynamics becomes confined into two regions in the top and bottom of the section.

As the value of  $L$  increases, the orbit of either  $S_1$  or  $S_3$  (depending on the initial conditions and consequently on the particular point on the section) approaches the one of  $S_2$ . For example, in Fig. 7 we can see two regular orbits with symmetric configurations for  $L = -0.05$  in the top panels. The first one corresponds to  $(\phi_1, J_1) \simeq (\pi, 0.03)$  and it is close to the lower symmetric stable periodic orbit while the other corresponds to  $(\phi_1, J_1) \simeq (\pi, 0.23)$  and it is close to the upper symmetric stable periodic orbit as can be seen in Fig. 6. In the first figure we can see how the interaction of  $S_2$  and  $S_1$  affects their orbits, while in the second we can observe the same feature for the  $S_2$  and  $S_3$  vortices.

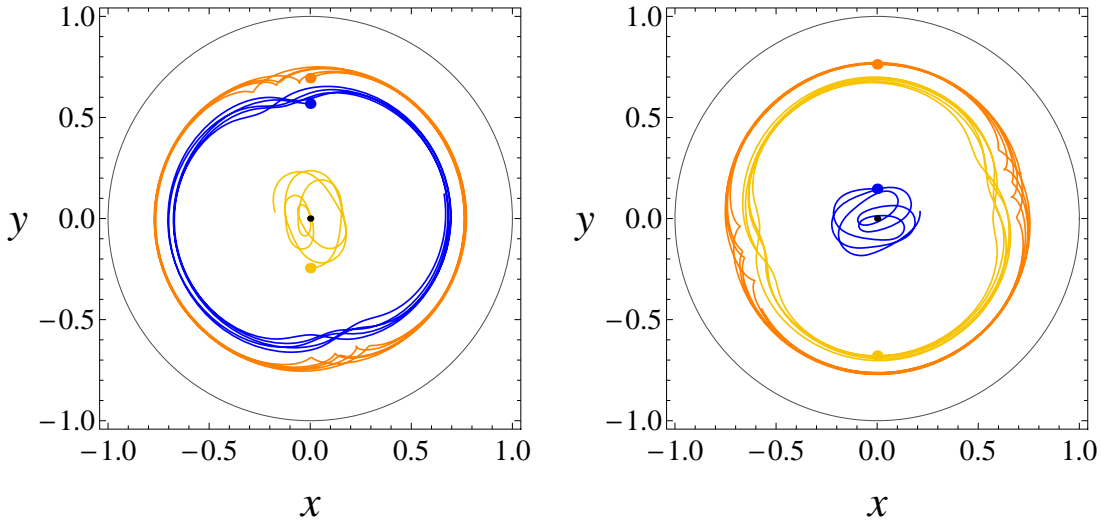


FIG. 7. (Color online) The form of two regular orbits in the  $(x - y)$  plane for  $L = -0.05$  and  $t = 15$ . In the left panel, the orbit which corresponds to  $(\phi_1, J_1) \simeq (\pi, 0.03)$  is depicted where the orbit of  $S_3$  approaches the one of  $S_2$ . In the right panel, the  $(\phi_1, J_1) \simeq (\pi, 0.23)$  is shown, where  $S_1$  approaches  $S_2$ .

### C. Dynamics for $L > 0$

As we progress into the predominantly chaotic phase space associated with positive values of  $L$ , the strong interaction between the vortices is responsible for the expansion of the chaotic region. The distinction of the motion in the  $(x - y)$  plane of an orbit which corresponds to a chaotic evolution in the Poincaré section is very clear from the one of the ordered orbits shown previously in the  $(x - y)$  plane. For example, in Fig. 8 the motion which corresponds to a chaotic orbit for  $L = 0.1$  is shown. In this case we can see how the orbits of the three vortices are mixing and filling the plane as time evolves, in contrast with the regular ones where the vortices occupy distinct regions in the  $(x - y)$  plane.

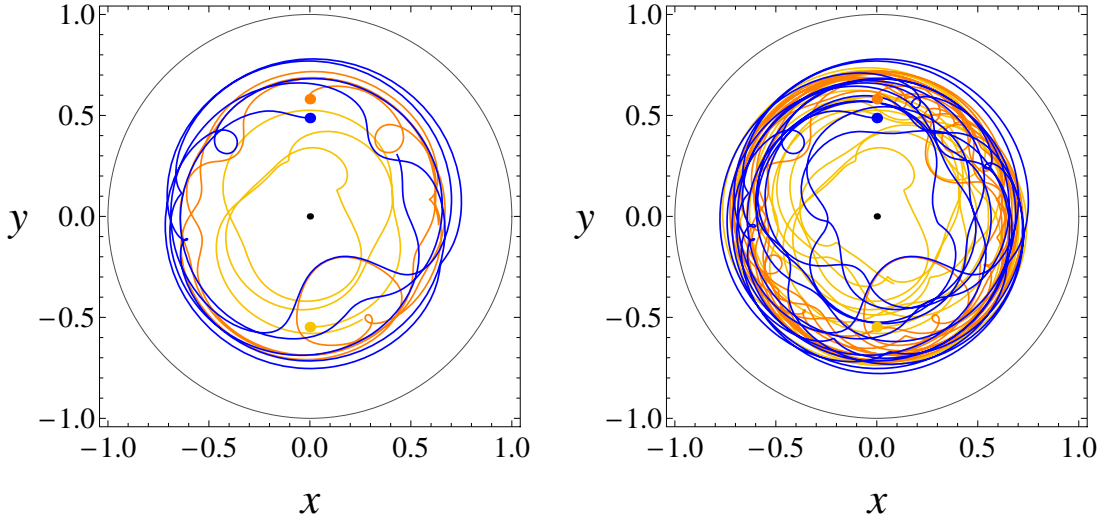


FIG. 8. (Color online) A chaotic mixing orbit for  $L = 0.1$  for  $(\phi_1, J_1) = (\pi, 0.15)$ . In the left panel, the orbit has evolved for  $t = 15$ , while in the right one for  $t = 50$ .

Although, the chaotic region grows larger and tends to occupy the whole phase-space for increasing values of  $L$ , there are two regular regions around  $\phi_1 = \pi$  which persist and apparently expand for a range of positive  $L$ 's beyond  $L > 0.05$ . These regions acquire their maximal size (i.e., fraction of the plane's area) close to the value of  $L = 0.25$  as can be seen in Fig. 9, before shrinking again for larger values of  $L$ .

Such features will be discussed in a more quantitative fashion in a forthcoming work [30].

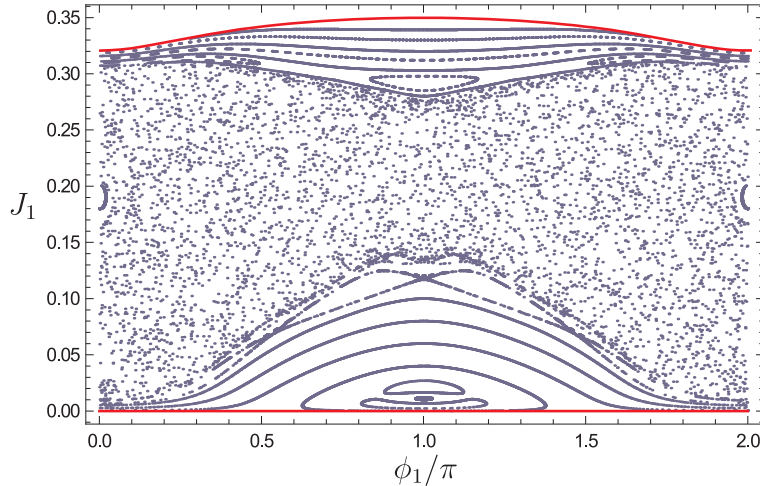


FIG. 9. (Color online) The Poincaré section for  $L = 0.25$ . In this area of values of  $L$ , the two persisting regular regions of the section have occupied their maximal area before shrinking again in size for larger  $L$ .

In addition to the expansion of the chaotic region, within the region  $0.2 < L < 0.247$ , an interesting bifurcation scenario unfolds. At  $L \simeq 0.2441$ , a period-doubling bifurcation of the stable symmetric periodic orbit which corresponds to  $(\phi_1, J_1) \simeq (\pi, 0.011)$  occurs and the stable orbit is replaced by an unstable (saddle point) one and an emerging stable one of double the original period. However, at  $L \simeq 0.2463$  an inverse period doubling bifurcation occurs, whereby the unstable periodic orbit becomes stable again giving rise to an extra asymmetric periodic orbit, which has double the period with respect to the original one. This way we end up with two stable symmetric periodic orbits one with double the period of the other and a doubled-period asymmetric unstable periodic orbit. The whole scenario can be seen in the panels of Fig. 10, while in those of Fig. 11 the corresponding eigenvalues of the Floquet matrix of the central periodic orbit are shown in the vicinity of  $-1$ , clearly illustrating the forward and reverse period-doubling bifurcation.

For  $L \simeq 0.3028$  a further significant structural change occurs. An asymmetric stable periodic orbit at  $(\phi_1, J_1) \simeq (0.505\pi, 0.101)$  appears through an inverse period doubling bifurcation. This is shown in detail in Fig. 12 through the Floquet multipliers of the relevant periodic orbit. In the left panel of Fig. 13 we can see the Poincaré section of the system for  $L = 0.35$ . We can distinguish the two additional regular regions around the asymmetric periodic orbit. Note that, from this value of  $L$  onward, the upper boundary of the section is calculated by the  $R_2 = 0$  requirement rather than the  $R_3 = 0$  that was used up to this point. This happens because as the value of  $L$  is increasing,  $R_2$  becomes smaller. Consequently, the  $S_2$  vortex becomes a candidate for crossing the center. The right panel of Fig. 13 shows the time evolution in the  $(x - y)$  plane of the asymmetric periodic orbits for this value of  $L$ .

In Fig. 14 the behavior of the system for  $0.365 \leq L \leq 0.43$  is shown. In the section which corresponds to  $L = 0.365$  we can see that the upper and the asymmetric regions of stability become wider, while in the lower region of stability the inverse bifurcation scenario of this described in Fig. 10 occurs, which leads the stable and unstable double-period and the stable single-period orbits to be replaced by a single-period orbit as it is shown in the surface of section for  $L = 0.37$ . For higher values of  $L$  we see that the area of the permitted orbits in the Poincaré section “shrinks”, i.e. the two boundary-curves approach around  $\phi_1 = \pi$  due to the energy and angular momentum conservation constraints. At the same time, we see how the region around the lower symmetric periodic orbit is “squeezed” by the boundary, and finally for  $L = 0.43$  disappears.

In Fig. 15 we see how the two asymmetric regions are combined in order to form a single central region. Actually, in the Poincaré sections for  $L = 0.44$  and  $L = 0.45$  we can see how the asymmetric periodic orbit is generated by the interaction of the invariant curve with the boundary. As the value of  $L$  is increased, both the lower and upper regions of ordered dynamics become extinct for  $L = 0.47$ . In what follows, we can observe, in the sections for  $L = 0.473$  and  $L = 0.49$ , how the section is separated in two parts. Due to the cyclic nature of the  $\phi_1$  variable, rather than being separated, the section is concentrated around  $\phi_1 = 0$ . Finally, as can be seen from the section for  $L = 0.55$ , all trajectories become regular and are

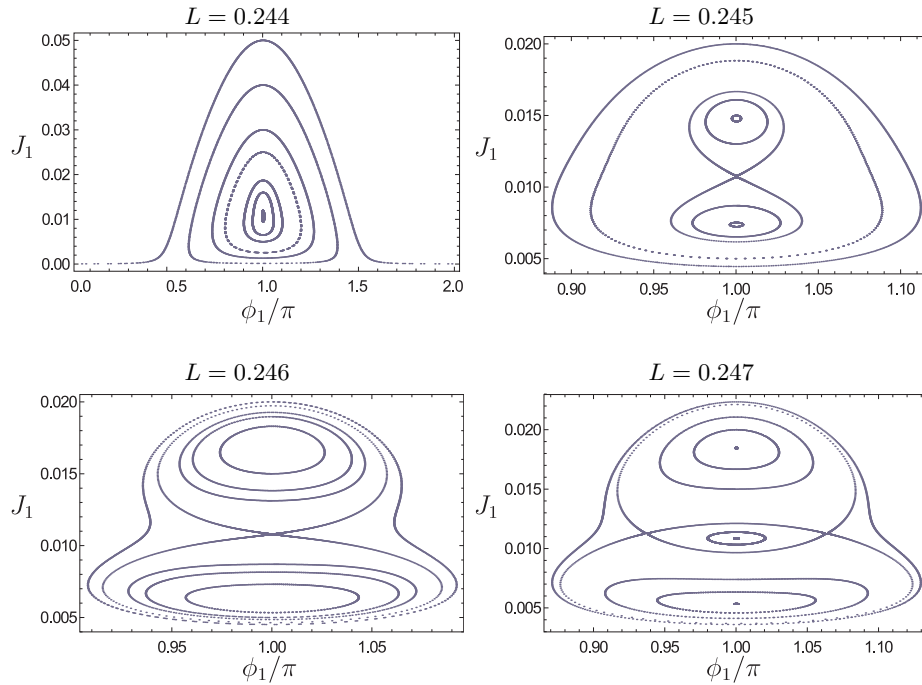


FIG. 10. (Color online) A magnification of the Poincaré sections is shown for the period doubling scenario described in the text and occurring for  $0.2 < L < 0.247$ .

confined around the collision orbit in order to present a near integrable picture.

#### D. Dynamics in different energy levels

The whole study has been focused so far on the value of the energy  $h = -0.7475$ . This energy has been chosen as a “characteristic” one since it corresponds to a typical vortex configuration. By the term typical, we mean here a configuration where the vortices are neither too close to each other, nor too close to the Thomas-Fermi radius of the condensate. By considering other values of the energy, e.g. in the range  $-1.1 \leq h \leq -0.5$ , which are physically meaningful, we observed qualitatively the same behavior of the system by varying the value of  $L$ . For low values of  $L$  the system is fully organized having regular orbits. For some value of  $L$  the central periodic orbit is getting destabilized through a pitchfork bifurcation, and a chaotic region is created. This region is getting wider as  $L$  increases. For even larger values of  $L$ , the permitted area of the Poincaré section shrinks and finally all the permitted configurations of the system correspond to regular orbits which are concentrated around the  $S_1 - S_3$  collision orbit. In general we can summarize the behavior of the system by mentioning that the motion of the system is regular when the initial configuration is close to the one or two-vortex regimes which correspond to the integrable cases of having just one or two vortices consisting the system. By one vortex regime here we mean a configuration where the three vortices are far enough from each other so that the interaction between them is weak. On the other hand by two-vortex regime we imply the configuration where two vortices are interacting strongly but are well separated from the third. Finally, when the motion of each vortex is strongly affected by its interaction with both of the other two, then the majority of the orbits are chaotic.

## IV. COMPARISON OF THE ODE MODEL WITH PDE COMPUTATIONS

One natural question that arises concerns the validity of our ODE model conclusions in connection to the full system. In particular, while the validity of our particle approach in some regular region of the system’s parameter space may be reasonable to expect, it is, arguably, a more bold assumption in the regimes where chaotic dynamics is predicted. It is in that light that we hereafter present a comparison of our results at the ODE level with the full Gross-Pitaevskii equation (GPE) model i.e., the corresponding

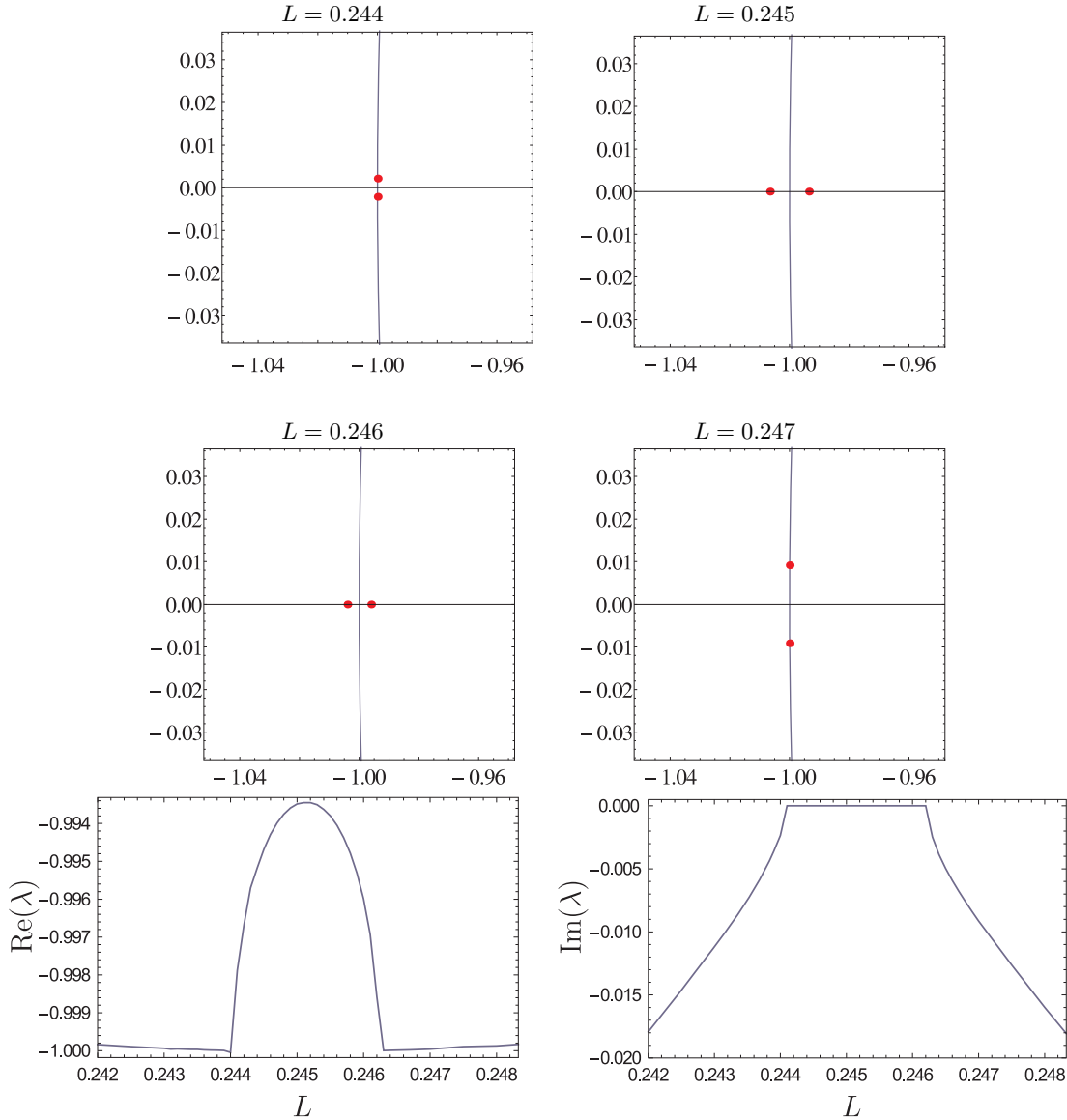


FIG. 11. (Color online) Top two rows: the dependence of the relevant Floquet multipliers of the destabilizing and restabilizing periodic orbit associated with the period doubling scenario described in the text. Bottom row: the real and imaginary parts of the associated multipliers.

PDE model.

The results of our comparison are shown in Fig. 16. In all 3 cases shown (a subset of a larger number of simulations performed –see also the discussion below–), consistently the same colors i.e. yellow, orange and blue (light, intermediate and dark grey) have been used to illustrate the 3 different vortices. Additionally, in all cases, the solid lines have been used to denote the ODE results, while the symbols (triangles, squares and circles) have been used to illustrate the corresponding PDE ones. Furthermore, the evolution has been given up to  $t = 500$  in both ODE and PDE and represented in the  $x - y$  plane of the dynamics.

At the PDE level, the GPE solved is of the form:

$$iu_t = -\frac{1}{2}\Delta u + V(r)u + (|u|^2 - \mu)u \quad (11)$$

is used. Here, the parabolic trapping potential is of the form  $V(r) = (1/2)\Omega^2 r^2$ . The parameters used here are  $\mu = 16.1$  and  $\Omega = 0.3538$ , which correspond to the experimental setup used in [20–22]. It should be noted here that for the comparison of the evolution of (11) with the ODE model, the original equations (2, 3) have been used. In addition, in order to quantitatively compare the particle model to the PDE one,

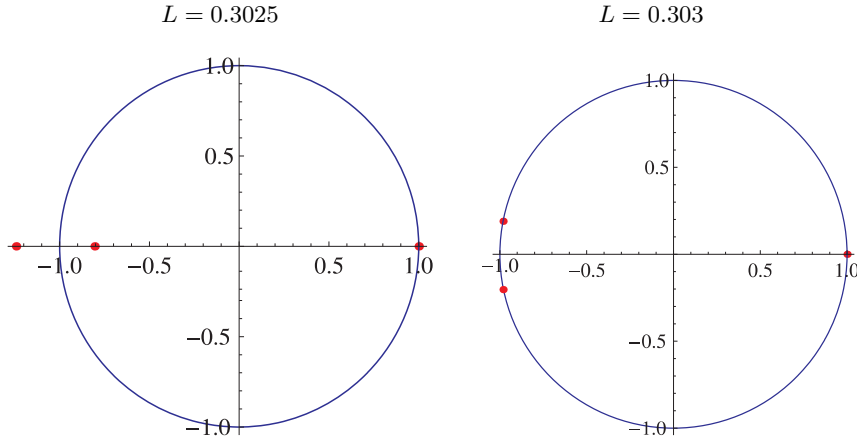


FIG. 12. (Color online) The Floquet multipliers for the inverse period doubling scenario of the asymmetric periodic orbit which leads to its stabilization.

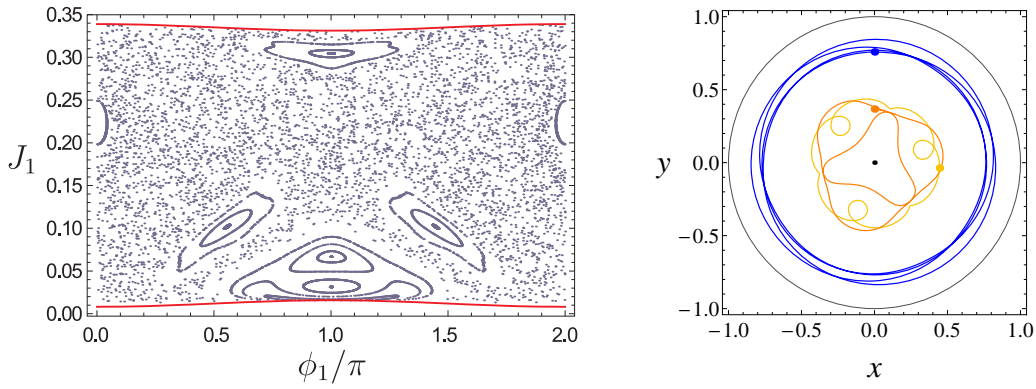


FIG. 13. (Color online) Left panel: the Poincaré section for  $L = 0.35$ . We can observe the two additional regions of regular orbits around the asymmetric double period periodic orbit. Right panel: the form of the asymmetric periodic orbits in the  $(x - y)$  plane is shown.

a slight technical modification was used (in comparison to Eqs. (5), namely  $\omega_{\text{pr}}(r) = \omega_{\text{pr}^0}/(1 - \alpha r^2)$  with  $\alpha = 0.78$  was used as for large distances from the trap center (which some of our trajectories entailed), this has been found to yield a slightly more accurate description of the precession frequency of an isolated vortex precessing around the trap center.

The first orbit shown corresponds to a highly regular trajectory in the case of  $L = -0.25$  whereby one of the vortices (the one with negative charge) is rotating fast in the periphery of the cloud, while the other two (positively charged ones) rotate close to the center. The second orbit still pertains to the same angular momentum, but clearly the relevant trajectory is more complex (yet still regular) involving a more pronounced quasi-periodic character. Finally, the third orbit is for  $L = -0.05$ , in this case existing within the (weakly) chaotic regime of the dynamics.

A common conclusion from all the cases is that while the 3-degree-of-freedom ODE model does not provide a perfect match for its infinite dimensional PDE counterpart, nevertheless, it provides a rather accurate prediction of the resulting motion for *all* of the above cases. This encompasses even complex dynamical features such as the meandering present in the quasi-periodic motion of the second orbit. Notice that in cases like the third weakly chaotic orbit of higher angular momentum, the trajectory may appear slightly less accurate than the earlier, more regular cases. Nevertheless, it still captures the gross features of the dynamics and the apparently (and gradually) space filling nature of the chaotic trajectories of the vortices.

There are numerous reasons as to why the agreement may not be more quantitatively accurate. Perhaps the most important one is that indeed we are approximating the infinite degree of freedom PDE with a 3 degree of freedom, far simpler dynamical system. Admittedly, we may not capture all of the dynamical features of the former within the latter (especially so in the current Hamiltonian realm). Weak sound

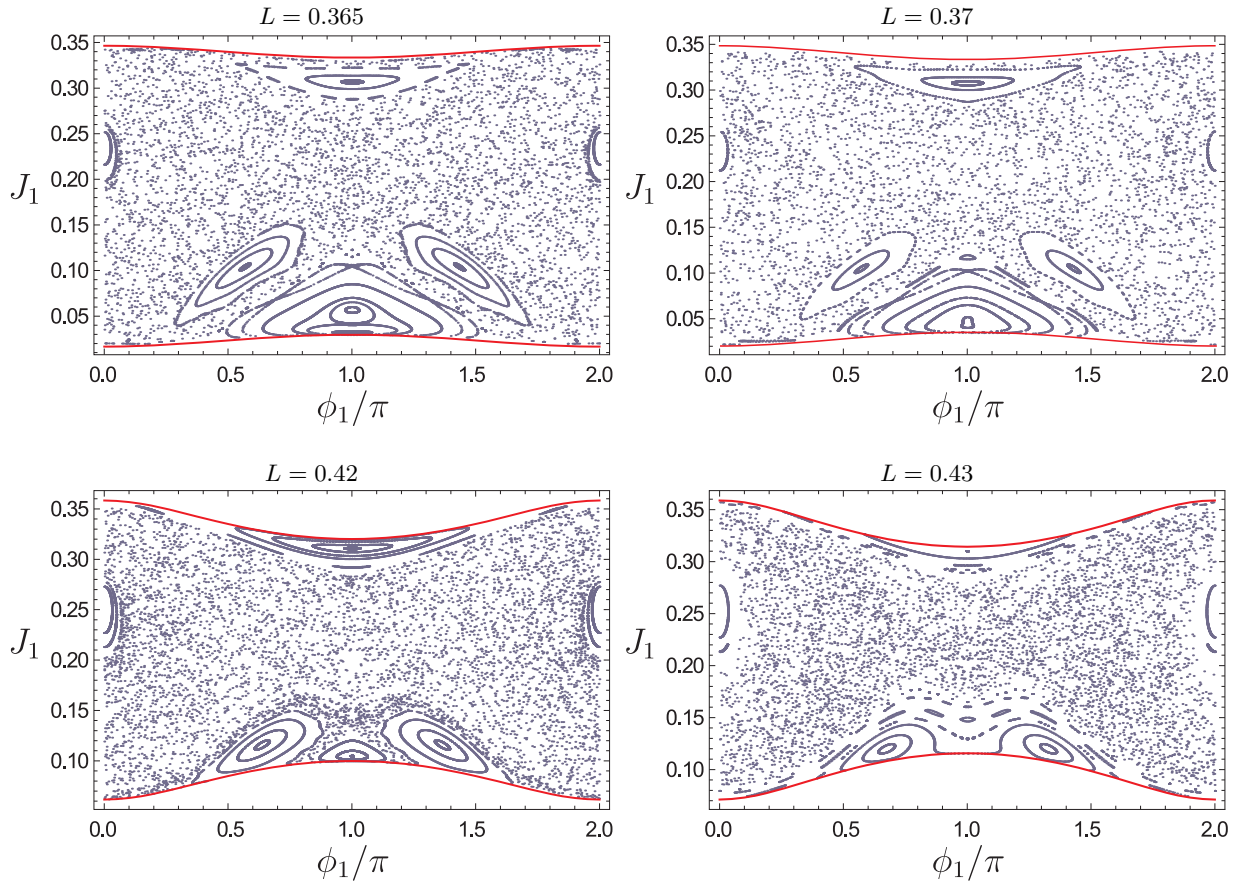


FIG. 14. (Color online) The Poincaré sections are shown in a similar way as in the earlier figures but now for  $0.365 \leq L \leq 0.43$ .

waves can be generated (and are indeed rather unavoidable in our initialization); these waves create weak interference and reflection features that slightly affect the vortex trajectories. Additionally, there are slight inaccuracies in the tracking of the vortex trajectories, importantly the vortices are not purely point particles, and finally the screening effect of the inter-vortex interaction is not fully captured in our dynamical model (among other things). Nevertheless, all these issues considered, and exactly because of their weak nature, the particle model still provides us with a very accurate qualitative predictor of the dynamics, remarkably, even when the latter is chaotic (already at the level of the 3 degree of freedom system) and hence presenting a sensitive dependence on its initial conditions.

Admittedly, this last feature becomes progressively more important, the stronger the chaoticity of the trajectories. Indeed, for completeness we should note here that we also considered highly chaotic trajectories e.g. for  $L = 0.25$ . In some such cases, we observed a substantial departure of the ODE trajectories from the corresponding PDE ones. However, we would argue that such a feature is rather reasonable to expect, given the especially sensitive nature of the corresponding examples to initial conditions. Broadly speaking, we believe that our finding that both ordered and even weakly chaotic trajectories can be adequately followed by the ODE model in a semi-quantitative fashion for long evolution times such as  $t = 500$  herein, lends the necessary credibility to our model and to its findings regarding the existence of such trajectories and the separation of regular from chaotic regions, which is one of the principal features of our analysis.

## V. CONCLUSIONS

In this work we have provided a detailed study of a dynamical system which describes the motion of three interacting vortices in a confined Bose-Einstein condensate. The vortices under consideration are

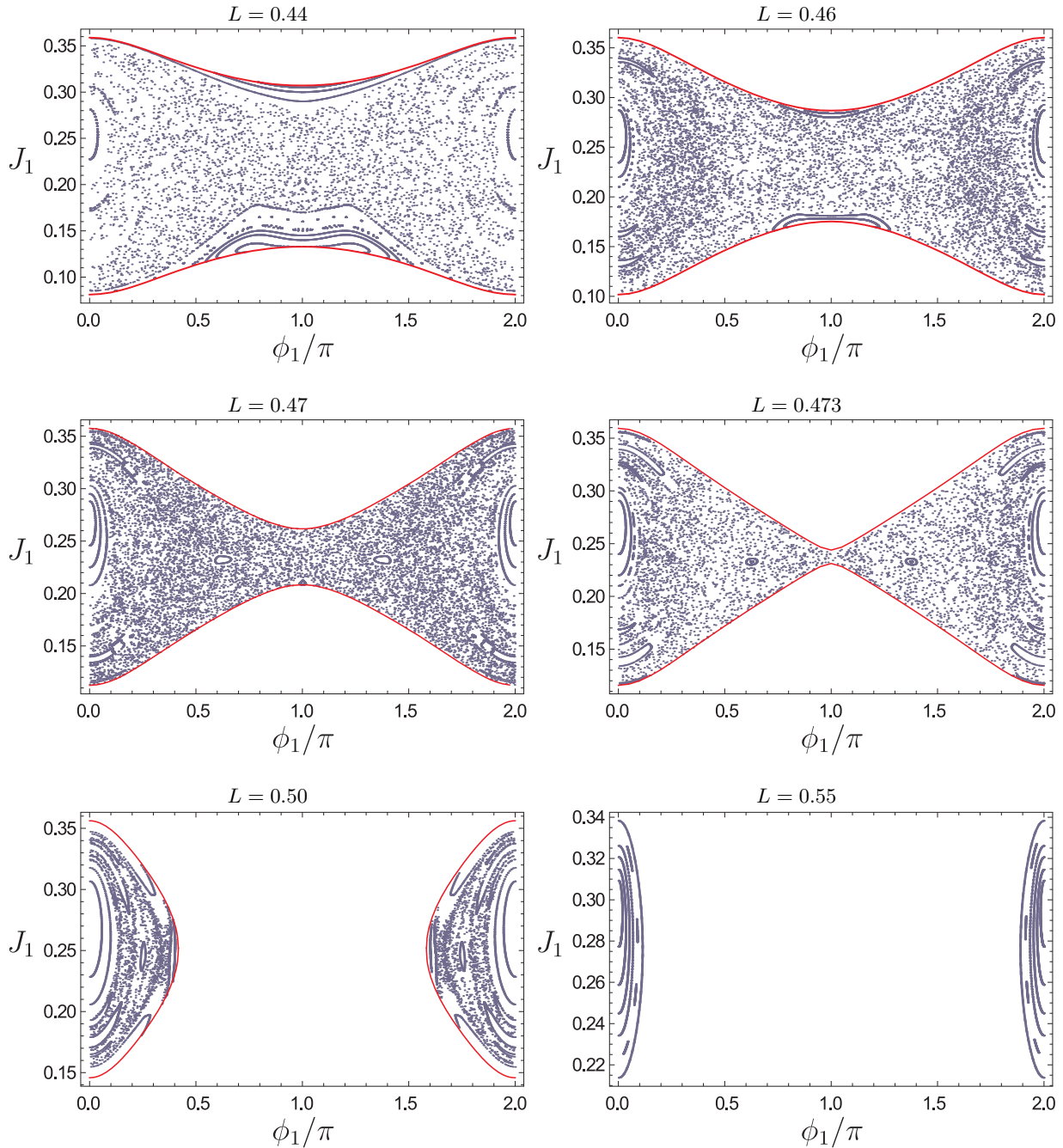


FIG. 15. (Color online) The Poincaré sections are shown for  $0.44 \leq L \leq 0.55$

non-co-rotating, with two of them having positive charge  $S_1 = S_3 = 1$  while the remaining having negative charge  $S_2 = -1$ . This system can be studied as a Hamiltonian system of three degrees of freedom, having two integrals of motion; the energy  $H$  and the angular momentum  $L$ . By applying suitable canonical transformations we can bring it to a reduced form of two degrees of freedom with  $L$  as a parameter. In order to study this system we numerically construct a series of Poincaré sections for varying  $L$ .

Our results show that for small values of the angular momentum the system behaves regularly, showing two qualitatively different regions in the phase space. One around a stable periodic orbit and the other around a collision orbit. This means that all the permitted configurations correspond to regular orbits. As  $L$  increases, chaotic orbits begin to exist. As the value of  $L$  increases further, the region of chaotic motion grows larger but there are always islands of regularity of significant area. As the value of  $L$  increases

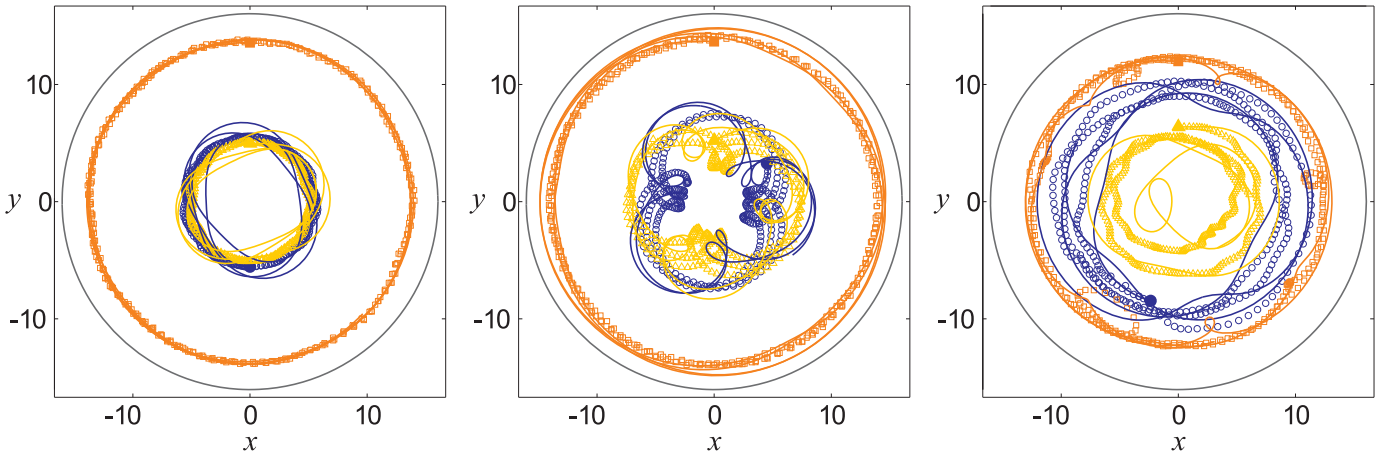


FIG. 16. (Color online) Comparison of vortex trajectories in the case of highly regular (top), less regular but still non-chaotic (middle) and finally in the case of a weakly chaotic trajectory. The solid lines indicate the ODE results, while the corresponding symbols the PDE ones. The grey circle denotes the Thomas-Fermi radius.

further, the area of permitted orbits of the system on the section decreases. For some value of  $L$ , it also becomes disconnected and finally it concentrates to a small area around the collision orbit where all the permitted configurations correspond to regular orbits and the system exhibits a behavior close to the one of an integrable one. Although the full study has been presented for a specific value of the energy, we have traced, by performing the same systematic exploration for other values of the energy, the principal features that are rather global in this three-vortex system.

This study may be considered as a starting point for a more detailed examination of ordered and chaotic features of multi-vortex cluster dynamics in isotropic (and possibly also anisotropic) Bose-Einstein condensates. Generalizing relevant notions to coherent structures of higher dimensions such as vortex-rings [31] in three-dimensional Bose-Einstein condensates [32] would also be a direction of interest for future work. Such studies will be reported in future publications.

#### ACKNOWLEDGMENTS

In this research, V.K. and G.V. have been co-financed by the European Union (European Social Fund - ESF) and Greek national funds through the Operational Program "Education and Lifelong Learning" of the National Strategic Reference Framework (NSRF) - Research Funding Program: THALES. Investing in knowledge society through the European Social Fund. V.K. would also like to thank the research committee of the Aristotle University of Thessaloniki for its support through the postdoctoral research award "Aristeia".

P.G.K. gratefully acknowledges support from US NSF via grants DMS-0806762, CMMI-1000337, from the Binational Science Foundation through grant 2010239, from the US AFOSR through grant FA9550-12-1-0332.

The authors are particularly thankful to Ricardo Carretero-González for relaying the relevant parameters, as well as for technical assistance in connection to the PDE numerical computations. Finally, the authors would also like to thank Nikos Kyriakopoulos for his valuable remarks.

- 
- [1] W.T. Kelvin, *Mathematical and Physical Papers* Cambridge University Press, 1878, Vol. IV, p. 135.
  - [2] T. Havelock, *Philos. Mag.* **11**, 617 (1931).
  - [3] L. Campbell and R. Ziff, Los Alamos Scientific Laboratory Report No. LA-7384-MS (1978).
  - [4] H. Aref, D. Vainchtein, **392**, 769 (1998).
  - [5] H. Aref, P. Newton, M. Stremler, T. Tokieda, D. Vainchtein, *Advances in applied Mechanics* **39**, 1 (2003).
  - [6] P. Newton, *The N-vortex problem: analytical techniques*, Springer-Verlag (New York, 2001).
  - [7] E. Yarmchuk, M. Gordon, and R. Packard, *Phys. Rev. Lett.* **43**, 214 (1979).

- [8] D. Durkin, and J. Fajans, *Phys. Fluids* **12**, 289 (2000).
- [9] B. Grzybowski, H. Stone, and G. Whitesides, *Nature* **405**, 1033 (2000); B. Grzybowski, H. Stone, and G. Whitesides, *Proc. Nat. Acad. Sci.* **99**, 4147 (2002).
- [10] A. Barry, G. Hall, and C.E. Wayne, *J. Nonlin. Sci.* **22**, 63 (2012).
- [11] Y. Chen, T. Kolokolnikov, D. Zhirov, *Proc. Roy. Soc. A* **469**, 20130085 (2013).
- [12] A. L. Fetter and A. A. Svidzinsky, *J. Phys.: Condens. Matter* **13**, R135 (2001).
- [13] A. L. Fetter, *Rev. Mod. Phys.* **81**, 647 (2009).
- [14] C. J. Pethick and H. Smith, *Bose-Einstein Condensation in Dilute Gases* (Cambridge University Press, Cambridge, 2002).
- [15] L. Pitaevskii and S. Stringari, *Bose-Einstein Condensation* (Oxford University Press, Oxford, 2003).
- [16] P. G. Kevrekidis, D. J. Frantzeskakis and R. Carretero-Gonzalez, *Emergent Nonlinear Phenomena in Bose-Einstein Condensates* (Springer-Verlag, Berlin, 2008).
- [17] P. K. Newton and G. Chamoun, *SIAM Review* **51**, 501 (2009).
- [18] Y. Castin and R. Dum, *Eur. Phys. J. D* **7**, 399 (1999).
- [19] K. W. Madison, F. Chevy, W. Wohlleben, and J. Dalibard *Phys. Rev. Lett.* **84**, 806 (2000).
- [20] D. V. Freilich, D. M. Bianchi, A. M. Kaufman, T. K. Langin, and D. S. Hall, *Science* **329** (2010) 1182.
- [21] S. Middelkamp, P.J. Torres, P.G. Kevrekidis, D.J. Frantzeskakis, R. Carretero-González, P. Schmelcher, D.V. Freilich, and D. S. Hall, *Phys. Rev. A* **84**, 011605(R) (2011).
- [22] R. Navarro, R. Carretero-Gonzalez, P.J. Torres, P.G. Kevrekidis, D.J. Frantzeskakis, M.W. Ray, E. Altuntas, D.S. Hall, *Phys. Rev. Lett.*, in press (2013); arXiv:1302.6612.
- [23] T. W. Neely, E.C. Samson, A.S. Bradley, M.J. Davis, and B. P. Anderson, *Phys. Rev. Lett.* **104**, 160401 (2010).
- [24] J.A. Seman, E. A. L. Henn, M. Haque, R. F. Shiozaki, E.R.F. Ramos, M. Caracanhas, P. Castilho, C. Castelo Branco, P.E.S. Tavares, F.J. Poveda-Cuevas, G. Roati, K.M.F. Magalhaes, and V.S. Bagnato, *Phys. Rev. A* **82**, 033616 (2010).
- [25] R.L. Jerrard, D. Smets, arXiv:1301.5213.
- [26] S. Middelkamp, P. G. Kevrekidis, D. J. Frantzeskakis, R. Carretero-González, and P. Schmelcher, *Phys. Rev. A* **82**, 013646 (2010).
- [27] S. McEndoo and Th. Busch *Phys. Rev. A* **79**, 053616 (2009).
- [28] H. Pu, C. K. Law, J. H. Eberly, and N. P. Bigelow *Phys. Rev. A* **59**, 1533 (1999).
- [29] A. J. Lichtenberg and M. A. Lieberman, *Regular and Chaotic Dynamics*, no. 38 in Applied Mathematical Sciences (Springer-Verlag, New York, NY, 1992), 2nd ed.
- [30] N. Kyriakopoulos, V. Koukouloyannis, Ch. Skokos and P. G. Kevrekidis, arXiv:1312.2542 [nlin.CD]
- [31] M. Konstantinov, *Phys. Fluids* **6**, 1752 (1994).
- [32] S. Komineas, *Eur. Phys. J. Special Topics* **147**, 133 (2007).